Localization Lengths over Metal to Band Insulator Transitions

N.D.M. Hine and W.M.C. Foulkes

Department of Physics, Imperial College London, Exhibition Road, London SW7 2AZ, United Kingdom

Abstract. Density functional and quantum Monte Carlo methods are used to examine the behaviour of the many-electron localization length near band insulator to metal transitions in various one- and two-dimensional model systems. The many-electron localization length is infinite in metals and finite in insulators, and is normally assumed to diverge as an insulator to metal transition is approached from the insulating side. Our results show that this is not the case: the band insulator to metal transition is normally first order and not associated with a diverging length scale. We also identify examples where the localization length diverges but the system is insulating on both sides of the divergence. The usefulness of the localization length as an indicator of the approach of an insulator to metal transition is therefore limited. A comparison of our quantum Monte Carlo and density functional results allows us to draw some general conclusions about the effect of correlation on localization.

PACS numbers: 71.23.An, 71.10.-w, 71.30.+h

1. Introduction

The question of whether the many-body wavefunction of a crystalline solid represents a metal or an insulator is easily answered for the determinantal wavefunctions used in one-electron band theory: if the density of one-electron states is finite at the Fermi level, the system is a metal; if not, it is an insulator. An alternative approach notes that one can apply a unitary transformation to the determinant of Bloch functions of an insulator to obtain an equivalent determinant of exponentially localized [1] one-electron Wannier functions. The exponential localization of the Wannier functions implies a corresponding exponential localization of the one-electron density matrix $\rho(\mathbf{r}, \mathbf{r}')$ as a function of $\mathbf{r} - \mathbf{r}'$, and it has been shown [2] that any system for which the second moment of $\rho(\mathbf{r}, \mathbf{r}')$ is finite must be insulating.

In the one-electron theory of disordered systems, the energy eigenfunctions may be localized and a finite density of states at the Fermi level need not imply conducting behaviour, but the more general idea that insulating behaviour results from wavefunction localization survives. In fact, more than forty years ago, Kohn [3] argued that *all* metal to insulator transitions, even those in strongly correlated interacting solids, are accompanied by a specific form of localization of the many-electron wavefunction $\Psi(\mathbf{r}_1, \mathbf{r}_2, \ldots, \mathbf{r}_N)$ in the configuration space of dN-dimensional vectors of the form $(\mathbf{r}_1, \mathbf{r}_2, \ldots, \mathbf{r}_N)$, where $\mathbf{r}_i$ is the d-dimensional position vector of electron i.

During the past decade, Kohn's approach has been substantially advanced by the development of the Berry-phase theory of polarization and localization [4, 5, 6, 7], which has allowed polarizations [8, 9], localization lengths [6, 7, 8], and dielectric constants [10] to be calculated in extended systems for the first time. These developments emerged from two tracks: studies of the properties and localization of Wannier functions [11]; and studies of polarization and the response of extended system to electric fields [4, 5, 12]. Both tracks led to similar conclusions about how to calculate the many-body localization length that determines whether a material is metallic or insulating.

These ideas were generalized and put on a firmer foundation by the work of Souza, Wilkens, and Martin [7], who used a generating function approach to provide expressions for polarizations and localization lengths in terms of the centre of mass of the many-body wavefunction. Under certain assumptions about the form of the many-body wavefunction, they also showed that their expressions agreed with those proposed by Resta and Sorella [6], and provided a link between the localization length and the conductivity as expressed by the Kubo formula, and thus between the localization length and the energy gap. Finally, they introduced the concept of a many-body Wannier function and linked it to Kohn's earlier suggestion [3] that "disconnectedness", identified as localization of the many-body wavefunction in configuration space, was an essential characteristic of the wavefunction of any insulator.

To date, there have been few applications of these ideas in a many-body context, mainly because it is difficult to carry out accurate many-body calculations for the very large system sizes required. Among the exceptions are two quantum Monte Carlo (QMC) studies, one of phase transitions in the one-dimensional ionic Hubbard model [13], and one of the dielectric response of periodic systems [9]. In the latter, it was observed that the inclusion of many-body correlation effects dramatically affected the value of the polarizability and improved its convergence with system size by decreasing the localization length, a conclusion supported by calculations in which self-interaction corrections were included in calculations of Born effective charges [14].

Section 2 of this article shows how the standard formulae for polarization and localization in many-body systems may be derived by considering the centre of mass and spread of the many-body Wannier functions. The many-body version of the modern theory of polarization is thus formulated in a manner analogous to King-Smith and Vanderbilt's original formulation [4, 5] of the non-interacting version. This is followed in Sec. 3 by a discussion of the assumption of short-ranged correlation required to evaluate these formulae in interacting many-electron systems. Section 4 looks at the evaluation of the localization length in systems of independent particles and addresses the relatively slow convergence with system size. In Sec. 5, we examine the behaviour of a series of simple models and describe the circumstances under which the approach of an insulator to metal transition is accompanied by a divergence of the localization length. Although finite and infinite values of the localization length distinguish metals from insulators, our density-functional theory (DFT) and QMC results show that the approach of an insulator to metal transition is rarely associated with a diverging localization length. We also show that the symmetry properties of the bands that cross at the transition strongly influence whether or not a divergence is seen. Appendix A discusses the evaluation of the localization length of a Slater determinant of orbitals expressed in a plane-wave basis, and Appendix B describes the behaviour of the statistical error associated with a measurement of the localization

length in a QMC simulation.

2. Localization Lengths and Many-Body Wannier Functions

2.1. Twisted boundary conditions

Because of the difficulty of dealing with wavefunctions of infinite numbers of variables, many-electron simulation methods such as QMC are always applied to finite systems and use periodic boundary conditions. We consider an N-electron simulation cell (preferably many times larger than the unit cell of the underlying crystal) with sides of length A_1, ..., A_d, where d is the spatial dimension. For simplicity, we assume that the simulation-cell lattice vectors $\mathbf{A}_1$, ..., $\mathbf{A}_d$ are orthogonal; the generalization to non-orthogonal simulation cells is straightforward but complicates the notation.

The periodic boundary conditions are imposed by insisting that the many-electron Hamiltonian be strictly periodic across the simulation cell. In other words, given any lattice vector $\mathbf{R} = (n_1 A_1, \ldots, n_d A_d)$, where n_1, ..., n_d are integers, we insist that

$$\hat{H}(\mathbf{r}_1, \ldots, \mathbf{r}_i + \mathbf{R}, \ldots, \mathbf{r}_N) = \hat{H}(\mathbf{r}_1, \ldots, \mathbf{r}_i, \ldots, \mathbf{r}_N) \; . \tag{1}$$

Real crystals do not possess this symmetry because the Coulomb interaction is not periodic, so we replace the Coulomb interaction with the periodic Ewald interaction. The finite size errors resulting from this replacement reduce as the simulation cell is made larger and the properties of the artificially periodic system tend to those of a real crystal.

Significantly, it is not necessary to insist that the N-electron wavefunction is periodic over the same simulation cell as the Hamiltonian. One can choose to solve the Schrödinger equation for Ψ within a larger "supercell" with sides $\widetilde{A}_\alpha = L_\alpha A_\alpha$ ($\alpha = 1, 2, \ldots, d$), where the L_α are positive integers and the wavefunction satisfies periodic boundary conditions across the supercell only. It is straightforward to show [19] that the energy eigenfunctions obtained via this procedure satisfy a version of Bloch's theorem,

$$\Psi_{\mathbf{k}}(\mathbf{r}_1, \ldots, \mathbf{r}_i + \mathbf{R}, \ldots, \mathbf{r}_N) = e^{i\mathbf{k}\cdot\mathbf{R}} \Psi_{\mathbf{k}}(\mathbf{r}_1, \ldots, \mathbf{r}_i, \ldots, \mathbf{r}_N) \; , \tag{2}$$

and may be labelled by a Bloch wave vector $\mathbf{k} = (m_1 \delta k_1, \ldots, m_d \delta k_d)$, where m_1, ..., m_d are integers and $\delta k_\alpha = 2\pi / \widetilde{A}_\alpha$. The phase factor $e^{i\mathbf{k}\cdot\mathbf{R}}$ is unchanged if the integer m_α is replaced by $m_\alpha + L_\alpha$, implying that the Bloch wavevector $\mathbf{k}$ may be chosen to lie in the first simulation-cell Brillouin zone. The total number $N_k = L_1 L_2 \ldots L_d$ of distinct Bloch wavevectors is then equal to the number of simulation cells in the supercell. Many-particle Bloch wavefunctions such as $\Psi_{\mathbf{k}}$ are often said to obey "twisted boundary conditions" and $\mathbf{k}$ is called the twist vector.

The antisymmetry of the many-fermion wavefunction ensures that the twist vector $\mathbf{k}$ is the same for every electron and so $\Psi_{\mathbf{k}}$ can be divided into a simulation-cell periodic part and a phase factor as

$$\Psi_{\mathbf{k}}(\mathbf{r}_1, \ldots, \mathbf{r}_N) = e^{i\mathbf{k}.\mathbf{X}} \, \Phi_{\mathbf{k}}(\mathbf{r}_1, \ldots, \mathbf{r}_N) \; , \tag{3}$$

where

$$\mathbf{X} = \sum_{i=1}^{N} \mathbf{r}_i \; . \tag{4}$$

In finite systems, $\hat{\mathbf{X}} = \sum_{i=1}^{N} \hat{\mathbf{r}}_i$ is proportional to the operator for the electronic dipole moment and we shall often call it the dipole operator from now on.

As in one-electron band theory, the wavefunction $\Psi_{\mathbf{k}}$ is only determined up to an arbitrary $\mathbf{k}$-dependent phase. For simplicity, we restrict our consideration to gauges in which $\Psi_{\mathbf{k}}$ is a differentiable function of $\mathbf{k}$ and $\Psi_{\mathbf{k}+\mathbf{G}} = \Psi_{\mathbf{k}}$ for all simulation-cell reciprocal lattice vectors $\mathbf{G}$. The most general gauge transformation preserving these properties takes the form

$$\Psi_{\mathbf{k}} \to e^{i\phi(\mathbf{k})}\Psi_{\mathbf{k}} \; , \tag{5}$$

where $\phi(\mathbf{k}) = \mathbf{k}\cdot\mathbf{R} - \beta(\mathbf{k})$, $\mathbf{R}$ is any simulation-cell lattice vector, and $\beta(\mathbf{k})$ is any periodic differentiable function of $\mathbf{k}$.

In one-electron theory, the use of Bloch's theorem reduces the solution of the Schrödinger equation for an infinite periodic crystal to the solution within a single unit cell subject to twisted boundary conditions. By averaging over twists (integrating over the Brillouin zone), the results for the infinite crystal are obtained exactly. The many-body version of Bloch's theorem described here is less powerful. Although the Schrödinger equation is solved within the supercell, the wavefunctions $\Psi_{\mathbf{k}}(\mathbf{r}_1, \ldots, \mathbf{r}_N)$ depend on the coordinates of the N electrons in one simulation cell only: the Hamiltonian is periodically repeated but the number of particles is not increased correspondingly. Averaging over twists reduces the finite-size errors in most cases but does not yield exact results for an infinite system.

The main reason for using twisted boundary conditions in many-electron theory is that the sensitivity of the system to the choice of twist vector provides useful information about its polarizability and conductivity. According to Ref. [20], the change in electronic polarization in response to some adiabatic change of Hamiltonian is equal to the change in the quantity

$$\mathbf{P}_{\mathrm{el}} = \frac{iq_e}{(2\pi)^3}\int d\mathbf{k}\,\langle\Phi_{\mathbf{k}}|\boldsymbol{\partial}_{\mathbf{k}}\Phi_{\mathbf{k}}\rangle \; , \tag{6}$$

where $\boldsymbol{\partial}_{\mathbf{k}} = (\partial_{k_1}, \ldots, \partial_{k_d}) = (\partial/\partial k_1, \ldots, \partial/\partial k_d)$ is the gradient operator in k space and q_e is the electronic charge. In Ref. [7], Souza, Wilkens and Martin showed using the fluctuation-dissipation theorem that the squared localization length in the α direction, defined by

$$\langle r_\alpha^2\rangle_c = \frac{-1}{NV_k}\int d\mathbf{k}\left[\langle\Phi_{\mathbf{k}}|\partial_{k_\alpha}^2\Phi_{\mathbf{k}}\rangle - \langle\Phi_{\mathbf{k}}|\partial_{k_\alpha}\Phi_{\mathbf{k}}\rangle\langle\Phi_{\mathbf{k}}|\partial_{k_\alpha}\Phi_{\mathbf{k}}\rangle\right] \; , \tag{7}$$

where $V_k = (2\pi)^3/V$ is the volume of the simulation-cell Brillouin zone, is proportional to a frequency integral of the conductivity tensor. In particular, the system is insulating if $\langle r_\alpha^2\rangle_c$ is finite and metallic if $\langle r_\alpha^2\rangle_c$ is infinite. The aim of the rest of this section is to provide a physical interpretation of these results by showing how $\mathbf{P}_{\mathrm{el}}$ and $\langle r_\alpha^2\rangle_c$ are related to the centres and quadratic spreads of the many-electron Wannier functions. The many-electron theory of polarization and localization is thus expressed in the same language as the one-electron theory developed by King-Smith and Vanderbilt [4, 5].

2.2. Many-body Wannier functions

Assuming that the system is insulating for all choices of twist vector $\mathbf{k}$, so that the ground state $\Psi_{\mathbf{k}}$ at each $\mathbf{k}$ is unique and clearly separated in energy from the excited states at that $\mathbf{k}$, we can use the Bloch-like form of Eq. (3) to define a set of many-body Wannier functions

$$W_{\mathbf{R}} = \frac{1}{\sqrt{N_k}}\sum_{\mathbf{k}} e^{-i\mathbf{k}.\mathbf{R}}\Psi_{\mathbf{k}} \; . \tag{8}$$

Both $\Psi_{\mathbf{k}}$ and $W_{\mathbf{R}}$ are normalised over the d-dimensional supercell of volume $N_k V$, with normalisation integrals carried out over the corresponding dN-dimensional configuration space of volume $(N_k V)^N$. As explained by Souza, Wilkens and Martin [7], $W_{\mathbf{R}}(\mathbf{r}_1, \mathbf{r}_2, \ldots, \mathbf{r}_N)$ is localized in the d-dimensional space of values of $\mathbf{X} = \mathbf{r}_1 + \ldots + \mathbf{r}_N$ but not in the remaining $dN - d$ dimensions of the configuration space. If one starts at a configuration-space point $(\mathbf{r}_1, \ldots, \mathbf{r}_N)$ near the peak of $W_{\mathbf{R}=\mathbf{0}}$ and shifts each electron coordinate by a different lattice vector $\mathbf{R}_i$, the final point will be near the peak of $W_{\mathbf{R}}$, where $\mathbf{R} = \sum_i \mathbf{R}_i$.

As in the case of single-particle Wannier functions, gauge transformations of the type discussed in Sec. 2.1 affect the position and spread of the many-electron Wannier functions. Fortunately, it is well established that single-particle Wannier functions have various gauge-invariant properties, including the minimum possible spread. As we see below, many-body Wannier functions, localized in $\mathbf{X}$, behave in the same way.

2.3. Wannier centres and polarization

One way to find the centre of a many-body Wannier function would be to calculate its first moment $\langle W_{\mathbf{0}} | \hat{\mathbf{X}} | W_{\mathbf{0}} \rangle$. If the dipole operator $\hat{\mathbf{X}}$ is applied to a function obeying periodic boundary conditions, however, the result is not periodic and does not lie in the Hilbert space of the periodic system. As emphasised by Resta [23], this means that $\hat{\mathbf{X}}$ is not an admissible operator in periodic systems. To circumvent this problem, consider instead the operator

$$\hat{Q}_\alpha \;=\; \frac{\sin(\delta k_\alpha \hat{X}_\alpha)}{\delta k_\alpha} \;=\; \frac{\sin(\delta \mathbf{k}_\alpha \cdot \hat{\mathbf{X}})}{\delta k_\alpha} \tag{9}$$

where $\delta \mathbf{k}_\alpha = (0, \ldots, \delta k_\alpha, \ldots 0)$ is a vector of length δk_α in the α direction. When applied to a state such as $W_{\mathbf{0}}$, which we assume is sharply peaked near $\mathbf{X}$=$\mathbf{0}$, the action of $\hat{Q}_\alpha$ is approximately that of $\hat{X}_\alpha$. Unlike $\hat{X}_\alpha$, however, $\hat{Q}_\alpha$ is periodic across the supercell.

Using the definition of the Wannier function, Eq. (8), we find that

$$\begin{aligned}
\hat{Q}_\alpha \, |W_{\mathbf{0}}\rangle \;&=\; \frac{1}{\delta k_\alpha \sqrt{N_k}} \left(\frac{e^{i\delta \mathbf{k}_\alpha \cdot \hat{\mathbf{X}}} - e^{-i\delta \mathbf{k}_\alpha \cdot \hat{\mathbf{X}}}}{2i} \right) \sum_{\mathbf{k}} |\Psi_{\mathbf{k}}\rangle \\
&= \frac{-i}{2\delta k_\alpha \sqrt{N_k}} \left(e^{i\delta \mathbf{k}_\alpha \cdot \hat{\mathbf{X}}} \sum_{\mathbf{k}} |\Psi_{\mathbf{k}-\delta \mathbf{k}_\alpha}\rangle - e^{-i\delta \mathbf{k}_\alpha \cdot \hat{\mathbf{X}}} \sum_{\mathbf{k}} |\Psi_{\mathbf{k}+\delta \mathbf{k}_\alpha}\rangle \right) \\
&= \frac{i}{\sqrt{N_k}} \sum_{\mathbf{k}} e^{i\mathbf{k}\cdot\hat{\mathbf{X}}} \left(\frac{|\Phi_{\mathbf{k}+\delta \mathbf{k}_\alpha}\rangle - |\Phi_{\mathbf{k}-\delta \mathbf{k}_\alpha}\rangle}{2\delta k_\alpha} \right) \\
&= \frac{i}{\sqrt{N_k}} \sum_{\mathbf{k}} e^{i\mathbf{k}\cdot\hat{\mathbf{X}}} \Delta_{k_\alpha} |\Phi_{\mathbf{k}}\rangle \;,
\end{aligned} \tag{10}$$

where Δ_{k_α} is a discretized derivative with respect to k_α and the replacement of $\sum_{\mathbf{k}} |\Psi_{\mathbf{k}}\rangle$ by $\sum_{\mathbf{k}} |\Psi_{\mathbf{k}\pm\delta\mathbf{k}_\alpha}\rangle$ was possible because $|\Psi_{\mathbf{k}}\rangle$ is a periodic function of $\mathbf{k}$.

The expectation value of $\hat{Q}_\alpha$ in the many-body Wannier function centered on $\mathbf{R} = \mathbf{0}$ is given by

$$\langle W_{\mathbf{0}} | \hat{Q}_\alpha | W_{\mathbf{0}} \rangle = \frac{i}{N_k} \sum_{\mathbf{k}'} \sum_{\mathbf{k}} \left\langle \Phi_{\mathbf{k}'} \middle| e^{-i\mathbf{k}'.\hat{\mathbf{X}}} e^{i\mathbf{k}.\hat{\mathbf{X}}} \middle| \Delta_{k_\alpha} \Phi_{\mathbf{k}} \right\rangle . \tag{11}$$

Both $\Phi_{\mathbf{k}'}$ and $\Delta_{k_\alpha}\Phi_{\mathbf{k}}$ have the periodicity of the simulation cell and may be represented as dN-dimensional Fourier series involving simulation-cell reciprocal lattice vectors

only. Since $\mathbf{k}$ and $\mathbf{k}'$ lie in the simulation-cell Brillouin zone and hence cannot differ by a non-zero simulation-cell reciprocal lattice vector, it follows that every matrix element with $\mathbf{k} \neq \mathbf{k}'$ vanishes, leaving

$$\langle W_{\mathbf{0}} | \hat{Q}_\alpha | W_{\mathbf{0}} \rangle = \frac{i}{N_k} \sum_{\mathbf{k}} \left\langle \Phi_{\mathbf{k}} \middle| \Delta_{k_\alpha} \Phi_{\mathbf{k}} \right\rangle . \tag{12}$$

In the limit of very large supercells, and assuming a choice of gauge for which $\Phi_{\mathbf{k}}$ is a smooth function of $\mathbf{k}$, this becomes

$$\langle W_{\mathbf{0}} | \hat{Q}_\alpha | W_{\mathbf{0}} \rangle = \frac{i}{V_k} \int d\mathbf{k} \left\langle \Phi_{\mathbf{k}} \middle| \partial_{k_\alpha} \Phi_{\mathbf{k}} \right\rangle , \tag{13}$$

where $V_k = (2\pi)^3/V$ is the volume of the simulation-cell Brillouin zone. The one-electron version of this result was originally derived by Blount [18]. The matrix elements in Eq. (13) are evaluated by integration over the region of configuration space corresponding to the supercell, with both $W_{\mathbf{0}}$ and $\Phi_{\mathbf{k}}$ normalised to unity over that region. Since $\Phi_{\mathbf{k}}$ is periodic, however, the $\Phi_{\mathbf{k}}$ matrix element may also be evaluated by integration over the smaller region of configuration space corresponding to one simulation cell, as long as $\Phi_{\mathbf{k}}$ is normalised to unity over the smaller region instead.

Comparing Eq. (13) with Eq. (6), we see that $(P_{\mathrm{el}})_\alpha = q_e \langle W_{\mathbf{0}} | \hat{Q}_\alpha | W_{\mathbf{0}} \rangle / V$. The change in polarization in response to some adiabatic change of Hamiltonian may therefore be obtained from the change in the first moment of the many-body Wannier function $W_{\mathbf{0}}$, in analogy with the non-interacting case. A general periodic gauge transformation of the type defined in Eq. (5) shifts the right-hand side of Eq. (13) by the lattice vector $\mathbf{R}$, corresponding to a shift in the polarization by some integer multiple of the quantum of polarization [4, 5].

2.4. The spread functional and the localization length

A similar approach may be used to find the spread of the Wannier functions, from which we can calculate the localization length. Proceeding as above, we obtain

$$\hat{Q}_\alpha \hat{Q}_\beta \, | W_{\mathbf{0}} \rangle = -\frac{1}{\sqrt{N_k}} \sum_{\mathbf{k}} e^{i\mathbf{k}\cdot\mathbf{X}} \Delta_{k_\alpha} \Delta_{k_\beta} \, | \Phi_{\mathbf{k}} \rangle \ , \tag{14}$$

and hence the large supercell limit of the tensor spread functional

$$\Omega_{\alpha\beta} = \langle W_{\mathbf{0}} | \, \hat{Q}_\alpha \hat{Q}_\beta \, | W_{\mathbf{0}} \rangle - \langle W_{\mathbf{0}} | \, \hat{Q}_\alpha \, | W_{\mathbf{0}} \rangle \, \langle W_{\mathbf{0}} | \, \hat{Q}_\beta \, | W_{\mathbf{0}} \rangle \tag{15}$$

is

$$\begin{aligned} \Omega_{\alpha\beta} = \ - \Bigg(& \int \frac{d\mathbf{k}}{V_k} \left\langle \Phi_{\mathbf{k}} \middle| \partial_{k_\alpha} \partial_{k_\beta} \Phi_{\mathbf{k}} \right\rangle \\ & - \int \frac{d\mathbf{k}}{V_k} \int \frac{d\mathbf{k}'}{V_k} \left\langle \Phi_{\mathbf{k}} \middle| \partial_{k_\alpha} \Phi_{\mathbf{k}} \right\rangle \left\langle \Phi_{\mathbf{k}'} \middle| \partial_{k'_\beta} \Phi_{\mathbf{k}'} \right\rangle \Bigg) . \end{aligned} \tag{16}$$

Following Ref. [11], we split the spread functional into a gauge invariant part Ω_I and a gauge dependent part $\widetilde{\Omega}$, simply by choosing Ω_I to include the terms in which the phase $e^{i\phi(\mathbf{k})}$ cancels:

$$\Omega = \Omega_I + \widetilde{\Omega} \, , \tag{17}$$

where

$$(\Omega_I)_{\alpha\beta} = - \int \frac{d\mathbf{k}}{V_k} \Big(\langle \Phi_{\mathbf{k}} | \partial_{k_\alpha} \partial_{k_\beta} \Phi_{\mathbf{k}} \rangle - \langle \Phi_{\mathbf{k}} | \partial_{k_\alpha} \Phi_{\mathbf{k}} \rangle \langle \Phi_{\mathbf{k}} | \partial_{k_\beta} \Phi_{\mathbf{k}} \rangle \Big) \tag{18}$$

and

$$\widetilde{\Omega}_{\alpha\beta} = \int \frac{d\mathbf{k}}{V_k} \int \frac{d\mathbf{k}'}{V_k} \langle \Phi_{\mathbf{k}} | \partial_{k_\alpha} \Phi_{\mathbf{k}} \rangle \left(\langle \Phi_{\mathbf{k}'} | \partial_{k'_\beta} \Phi_{\mathbf{k}'} \rangle - \langle \Phi_{\mathbf{k}} | \partial_{k_\beta} \Phi_{\mathbf{k}} \rangle \right). \quad (19)$$

Thus we see that $(\Omega_I)_{\alpha\alpha} = N\langle r_\alpha^2 \rangle_c$, where $\langle r_\alpha^2 \rangle_c$ is the squared localization length in the α direction as defined in Eq. (7). Furthermore, by re-expressing the many-body Bloch functions in terms of the Wannier functions, the gauge-dependent part of the functional may be written as

$$\widetilde{\Omega}_{\alpha\beta} = \sum_{\mathbf{R}\neq\mathbf{0}} \left\langle W_{\mathbf{R}} | \hat{Q}_\alpha | W_{\mathbf{0}} \right\rangle \left\langle W_{\mathbf{0}} | \hat{Q}_\beta | W_{\mathbf{R}} \right\rangle . \quad (20)$$

If the many-body Wannier functions of an insulator are taken as "disconnected" Kohn's functions, it must be possible to choose a gauge in which those localized on different vectors $\mathbf{R}$ are non-overlapping in configuration space when the simulation cell is large enough. The gauge-dependent part of the spread therefore tends to zero with increasing simulation-cell size [7]. This allows us to limit our consideration to the gauge-invariant part Ω_I.

3. Evaluation of the Spread Functional

3.1. Discretization of the twist averaging

Before Ω_I can be evaluated numerically, the integral over $\mathbf{k}$ must be discretized again. We use the identity $\partial_{q_\alpha}^2 \ln f = \frac{1}{f}\partial_{q_\alpha}^2 f - \frac{1}{f^2}(\partial_{q_\alpha} f)^2$ with $f(\mathbf{q}) = \langle \Phi_{\mathbf{k}} | \Phi_{\mathbf{k}+\mathbf{q}} \rangle$ to rewrite $(\Omega_I)_{\alpha\alpha}$ as

$$(\Omega_I)_{\alpha\alpha} = -\frac{1}{V_k} \left[\int \mathrm{d}\mathbf{k}\, \partial_{q_\alpha}^2 \ln \langle \Phi_{\mathbf{k}} | \Phi_{\mathbf{k}+\mathbf{q}} \rangle \right]_{\mathbf{q}=\mathbf{0}} . \quad (21)$$

The discretized equivalent of this expression for the finite supercell containing $N_k = L_1 \ldots L_d$ simulation cells is

$$\begin{aligned}(\Omega_I)_{\alpha\alpha} = & -\frac{1}{V_k} \sum_{\mathbf{k}} \frac{V_k}{N_k} \frac{1}{\delta k_\alpha^2} \Big[\ln \langle \Phi_{\mathbf{k}} | \Phi_{\mathbf{k}+\delta\mathbf{k}_\alpha} \rangle \\ & + \ln \langle \Phi_{\mathbf{k}} | \Phi_{\mathbf{k}-\delta\mathbf{k}_\alpha} \rangle - 2 \ln \langle \Phi_{\mathbf{k}} | \Phi_{\mathbf{k}} \rangle \Big] , \end{aligned} \quad (22)$$

where $\partial_{q_\alpha}^2 f(\mathbf{q})$ has been approximated as $(f(\mathbf{q}+\delta\mathbf{k}_\alpha) + f(\mathbf{q}-\delta\mathbf{k}_\alpha) - 2f(\mathbf{q}))/(\delta k_\alpha)^2$. The final term in Eq. (22) is zero if $\Phi_{\mathbf{k}}$ is normalised to unity. The periodicity of the summand over the simulation-cell Brillouin zone allows us to make the substitution $\mathbf{k} \to \mathbf{k} + \delta\mathbf{k}_\alpha$ in the second term, which changes it from $\langle \Phi_{\mathbf{k}} | \Phi_{\mathbf{k}-\delta\mathbf{k}_\alpha} \rangle$ to $\langle \Phi_{\mathbf{k}+\delta\mathbf{k}_\alpha} | \Phi_{\mathbf{k}} \rangle$, giving

$$(\Omega_I)_{\alpha\alpha} = -\frac{1}{N_k} \sum_{\mathbf{k}} \frac{1}{\delta k_\alpha^2} \ln |\langle \Phi_{\mathbf{k}} | \Phi_{\mathbf{k}+\delta\mathbf{k}_\alpha} \rangle|^2 . \quad (23)$$

3.2. Ansatz wavefunction for a larger system

If one can solve the many-electron Schrödinger equation for a fine enough grid of twists and evaluate the overlaps of the wavefunctions at neighbouring twist vectors, Eq. (23) can be used directly. In other situations, however, it would be more convenient to be able to calculate the localization length from a single expectation value evaluated over a larger system. In this section, we use a variation of the argument of Refs.

[6, 7] to show how, by means of an ansatz about the form of the wavefunction for the larger system, the localization length can be related to a single expectation value of the "many-body phase operator" introduced by Resta [23].

In Sec. 2.1, we introduced a supercell containing $N_k = L_1 L_2 \dots L_d$ simulation cells. The Schrödinger equation for the N electrons in one simulation cell,

$$\hat{H}(\mathbf{r}_1, \dots, \mathbf{r}_N)\Psi(\mathbf{r}_1, \dots, \mathbf{r}_N) = E\Psi(\mathbf{r}_1, \dots, \mathbf{r}_N) \; , \tag{24}$$

was then solved subject to periodic boundary conditions within this larger region, corresponding to twisted boundary conditions across the smaller simulation cell. The resulting N-electron energy eigenfunctions were shown to satisfy a version of Bloch's theorem, so enabling us to define N-electron Wannier functions $W_{\mathbf{R}}(\mathbf{r}_1, \dots, \mathbf{r}_N)$, which were identified as the "disconnected" functions introduced by Kohn [3] and are believed to be exponentially localized in insulators. More precisely, $W_{\mathbf{R}}(\mathbf{r}_1, \dots, \mathbf{r}_N)$ is localized in that region of the dN-dimensional configuration space where the d-dimensional vector $\mathbf{X} = \mathbf{r}_1 + \dots + \mathbf{r}_N$ is close to $\mathbf{R}$. The exponential localization implies that the Hamiltonian matrix elements between neighbouring Wannier functions are exponentially small, and hence that the ground state energy of the simulation cell is exponentially insensitive to the choice of twist vector $\mathbf{k}$. This insensitivity to boundary conditions is a defining characteristic of the insulating state.

The supercell introduced in Sec. 2.1 is mathematically convenient but should not be viewed as a physical system; in particular, it contains the same number of electrons, N, as the smaller simulation cell. Suppose, however, that we now introduce a physical supercell system containing N_k simulation cells and $\widetilde{N} = N_k N$ electrons subject to periodic boundary conditions. The wavefunction $\widetilde{\Psi}(\mathbf{r}_1, \dots, \mathbf{r}_{\widetilde{N}})$ of this physical supercell is unknown, but the availability of N_k N-electron Bloch functions $\Psi_{\mathbf{R}}$ and the supposition that electron correlation in an insulator is a short ranged effect suggests an appealing Hartree-Fock-like ansatz. Labelling the N_k simulation cells using an integer index $c = 1, \dots, N_k$, we write, as in [6, 7],

$$\widetilde{\Psi}(\mathbf{r}_1, \dots, \mathbf{r}_{\widetilde{N}}) = \hat{A} \prod_{\mathbf{k}}^{N_k} \Psi_{\mathbf{k}}(\mathbf{r}_{N(c-1)+1}, \dots \mathbf{r}_{N(c-1)+N}) \; . \tag{25}$$

where $\hat{A}$ is the antisymmetrization operator. The ansatz assumes that the $\widetilde{N} = N_k N$ electrons in the supercell correlate in groups of N at a time, so that $\widetilde{\Psi}$ can be written as an antisymmetrised product of N_k different N-electron wavefunctions. If the Hamiltonian of the physical supercell were a sum of terms involving each group of N electrons separately, as in a non-interacting system, $\widetilde{\Psi}$ would be the exact ground state. In an interacting system $\widetilde{\Psi}$ is clearly inexact, but since each N-electron wavefunction $\Psi_{\mathbf{k}}$ was originally an allowable periodic wavefunction for a smaller section of the solid, we are effectively requiring that beyond some range L, the difference between the interactions between genuinely distinguishable electrons and between periodic copies of the same electron becomes negligible. As the number of electrons N in the simulation cell and the cell volume V increase, the importance of correlations of longer range than the size of the simulation cell should decrease and $\widetilde{\Psi}$ should become more accurate.

As in [6, 7], we evaluate the expectation value

$$z_N = \langle \widetilde{\Psi} | e^{-i\delta\mathbf{k}_\alpha \cdot \widetilde{\mathbf{X}}} | \widetilde{\Psi} \rangle \tag{26}$$

of the "many-body phase operator" $e^{-i\delta\mathbf{k}_\alpha \cdot \widetilde{\mathbf{X}}}$ in this ansatz wavefunction, where $\widetilde{\mathbf{X}} = \mathbf{r}_1 + \dots + \mathbf{r}_{N_k N}$. The overlap between two Slater determinants is the determinant of the

matrix of overlaps between the "orbitals", which here are N-electron wavefunctions labelled by a Bloch wavevector $\mathbf{k}$. This remains true even in this more complex many body case because any term in the antisymmetrization in which the same electron coordinate appears with different boundary conditions in the bra to those it has in the ket will vanish upon integration. We can thus write the expectation value as:

$$\left\langle \widetilde{\Psi} | e^{-i\delta\mathbf{k}_\alpha \cdot \widetilde{\mathbf{X}}} | \widetilde{\Psi} \right\rangle = \prod_{\mathbf{k}}^{N_k} \langle \Phi_{\mathbf{k}} | \Phi_{\mathbf{k}+\delta\mathbf{k}_\alpha} \rangle \ . \tag{27}$$

Comparing this result with Eq. (23), we see that

$$(\Omega_I)_{\alpha\alpha} = \frac{-1}{N_k(\delta k_\alpha)^2} \ln \left| \langle \widetilde{\Psi} | e^{-i\delta\mathbf{k}_\alpha \cdot \widetilde{\mathbf{X}}} | \widetilde{\Psi} \rangle \right|^2 , \tag{28}$$

and hence that the localization length $\langle r_\alpha^2 \rangle_c = (\Omega_I)_{\alpha\alpha}/N$ is given by

$$\langle r_\alpha^2 \rangle_c = \frac{-1}{\widetilde{N}(\delta k_\alpha)^2} \ln \left| \left\langle \widetilde{\Psi} \right| e^{-i\delta\mathbf{k}_\alpha \cdot \widetilde{\mathbf{X}}} \left| \widetilde{\Psi} \right\rangle \right|^2 . \tag{29}$$

This is Resta and Sorella's [6] result for the square of the localization length, or quadratic spread, in the α direction.

Equation (29) was originally obtained by supposing that the electron density could be decomposed into a sum of localized components, Fourier transforming, and applying the ansatz described above to produce a large enough system for convergence. This melds well with the proposed identification [7] of many-body Wannier functions with the "disconnected" parts of the many-body wavefunction hypothesised by Kohn [3]. Since the disconnected parts are non-overlapping in the configuration space of the electron coordinates, each can be considered as providing a separate contribution to the electron density in real space.

4. Convergence of the Localization Length with System Size

Previous studies [11, 6, 2] of electron localization in one-electron theories have noted the relatively slow and monotonically increasing convergence of the localization length as a function of system size. Sgiarovello, Peressi and Resta [2] examined the localization length $\langle x^2 \rangle_c$ in GaAs, and Marzari and Vanderbilt [11] the spread Ω of the maximally localized Wannier functions. Both came to similar conclusions.

The slow convergence can be explained by reference to Eq. (29) and consideration of the ansatz required to derive it. For the localization length to be well converged, the k-point sampling must be dense enough to sample the variation of the Bloch functions with $\mathbf{k}$; the finite difference approximation used in Eq. (23) is then a good approximation to the continuous k derivative in Eq. (21). Failure to converge with respect to $\delta\mathbf{k}_\alpha$ will appear as a variation of the localization length with the number of k points in the grid.

In one-electron theory, the convergence of Brillouin zone integrals may often be improved by shifting the entire grid of $\mathbf{k}$ vectors by a small amount $\widetilde{\mathbf{k}}$ relative to Γ. This corresponds to changing the strict periodic boundary conditions applied across the supercell to boundary conditions incorporating a twist vector $\widetilde{\mathbf{k}}$, which must be the same for all the orbitals. A supercell twist $\widetilde{\mathbf{k}} = \delta\mathbf{k}_\alpha$ shifts every $\mathbf{k}$ vector to one of its neighbours and is thus equivalent to a zero twist, implying that $\widetilde{\mathbf{k}}$ may be chosen to lie within the supercell Brillouin zone. The variation of the localization length with $\widetilde{\mathbf{k}}$ has not been investigated previously.

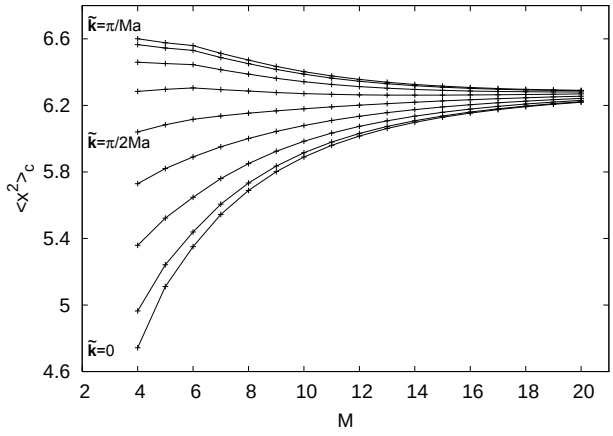

Figure 1. Convergence of the localization length (measured in Hartree atomic units) for a weakly bound but insulating array of quantum dots as a function of the size M of the $M \times M$ k-point grid. The lines join points calculated using the same supercell twist vector $\widetilde{\mathbf{k}}$. When the energy gap is small, convergence with supercell size Ma is very slow, especially for $\widetilde{\mathbf{k}} = \mathbf{0}$. In this particular system, the choice $\widetilde{\mathbf{k}} = \pi/(2Ma)$ yields the most rapid convergence.

To examine the convergence of the localization length, a two-dimensional array of potential wells capable of exhibiting a wide range of bandstructures was studied. The external potential consisted of a square array of Gaussian wells or "dots" of the form $V(\mathbf{r}) = -V_d \exp(-|\mathbf{r}-\mathbf{r}_c|^2/\rho^2)$, where $\mathbf{r}_c$ sets the center of the dot (in the center of the unit cell), ρ defines the width of the Gaussian, and V_d the dot depth. Neighbouring dots were separated by a distance a (the side of the unit cell, which is the same as the simulation cell in this case). The one-electron properties were treated within the framework of self-consistent density functional theory using the two-dimensional local density approximation from Ref. [21], and the wavefunctions were expressed in a basis of two-dimensional plane-waves limited by a cutoff energy E_{cut}, which was increased to convergence. The Bloch functions were calculated on an equally spaced grid of $M \times M$ k points within the Brillouin zone.

Figure 1 shows the localization length obtained by calculating z_N (see Eq. (26)) for a weakly bound array of dots, each containing six electrons and thus three filled bands of doubly-occupied states, for a range of $M \times M$ k-point grids offset by $\widetilde{\mathbf{k}}$ from the Γ point. Here and in the rest of this paper, numerical results are expressed in atomic units, with lengths measured in Bohr radii and energies in Hartrees. Details of the method used to evaluate z_N from the plane-wave representation of the orbitals are given in Appendix A. The parameters chosen were $\rho = 3$ and $a = 10$, with V_d tuned to a value only just yielding an insulating state with the first three bands fully occupied. If V_d is reduced further, the energy of the third band at $\mathbf{k} = (\frac{\pi}{a}, 0)$ becomes higher than that of the fourth band at $\mathbf{k} = (0, 0)$ and the system becomes metallic. The smallest energy gap is therefore indirect and the localization length might be expected to be only weakly dependent on the position of the grid, especially given that the total DFT energy is converged to five significant figures for $M \gtrsim 5$. However, as seen in Fig. 1, in this situation, chosen for its proximity to a transition, the convergence is slow and a 20×20 supercell is required to converge $\langle x^2 \rangle_c$ to 1%. A k-point grid centered on Γ

is seen to yield relatively slow convergence, in agreement with previous studies that have shown the same behaviour for total energies [19]. In this particular system, the most rapid convergence is achieved when $\widetilde{\mathbf{k}} = \pi/(2Ma)$.

5. Behaviour over Metal Insulator Transitions

Previous work [6] has indicated that the localization length correctly describes the various phases of a one-dimensional system of correlated electrons displaying a band insulator to Mott insulator transition with a metallic phase at the transition: a divergence is clearly observed in $\langle x^2 \rangle_c$ at sufficiently large system sizes. Given that the localization of Wannier functions is closely related to the energy gap, and that the localization length of a metal in band theory is always infinite, it might be supposed that the localization length would in general diverge as a metal-insulator transition is approached from the insulating side. As we shall show by a number of examples, however, this is not the case: the presence or absence of a divergence in one-electron theory depends on the nature of the bands that are crossing. The same behaviour is observed in many-electron quantum Monte Carlo simulations using a Slater-Jastrow trial function containing a Slater determinant of single-particle orbitals from band theory. To examine the behaviour of the localization length in a range of different situations, we study different arrangements of the two-dimensional quantum dot system introduced in Section 4.

5.1. Single dots in a quasi-one-dimensional chain

In this arrangement, the two-dimensional periodic array of dots is made quasi-one-dimensional by effectively isolating adjacent one-dimensional chains of dots. The unit cell is widened in the y direction and a strong barrier potential is introduced to separate adjacent unit cells in that direction. Every point on the k-space grid used for the Brillouin zone integration has $k_y = 0$, with equally spaced values of k_x. The simplicity of the one-dimensional bandstructure produced by this arrangement makes it easy to distinguish the effect of the symmetry properties of the Bloch functions on the behaviour of the localization tensor near the insulator-to-metal transition.

The lowest three eigenfunctions of an isolated dot that is not symmetric in the x and y directions can be classified as s-like, p_x-like and p_y-like: the s-like functions are nodeless, while the p_x- and p_y-like functions have nodes along the y- and x-axes, respectively, and change sign under reflections in those axes. The s- and p_x-like orbitals of a chain of dots oriented along the x axis mix to form hybrid bands, but the p_y-like orbitals mix only with each other and form a completely separate band. By varying the strengths of the confinement in the x- and y-directions independently, the p_y-like band can be shifted relative to the s and p_x bands. Starting from an insulating system with only the s and p_x bands occupied, this makes it possible to lower the energy of the p_y band until a band insulator to metal transition occurs.

We model this arrangement with a unit cell of size $a \times b$ and an asymmetric quartic potential of the form:

$$V(x,y) = \frac{1}{2}\omega_x^2 \left((x - a/2)^2 - \frac{2}{a^2}(x - a/2)^4 \right) + \frac{1}{2}\omega_y^2 \left((y - b/2)^2 - \frac{2}{b^2}(y - b/2)^4 \right) . \tag{30}$$

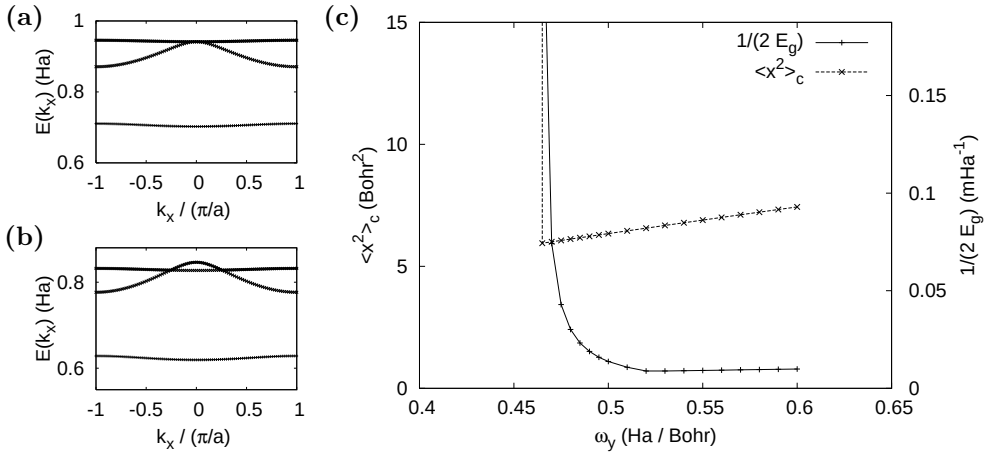

Figure 2. One-dimensional chain of 4-electron dots: **(a)** Energy bands $E(k_x)$ just before band crossing. Topmost flat band is p_y-like, middle is p_x-like, lowest is s-like. **(b)** Energy bands $E(k_x)$ shortly after transition. **(c)** Localization length $\langle x^2 \rangle_c$ and inverse direct energy gap $1/(2E_g)$ to lowest unoccupied state as ω is reduced.

By setting $\omega_y > \omega_x$ and $b > a$, we ensure there is an enormous barrier in the y direction, increasing the energy of the p_y band and creating a gap between the p_y band and the two s and p_x bands. Then, filling up the s and p_x bands, the Kohn-Sham equations are solved self-consistently for gradually lower values of ω_y until the upper p_y band falls to meet the higher of the s and p_x bands at $\mathbf{k} = 0$ and the energy gap reduces to zero (see Fig.2(a)). Because, by symmetry, there can be no matrix elements between states in the crossing bands, they cannot hybridize and the upper band has no effect on the lower until the moment at which they cross, at which point the lower band is no longer filled and the localization length becomes infinite. Beyond the transition, the bands pass straight through each other, remaining degenerate at the Fermi energy. Although at any k-point on the sampling grid the lowest three eigenvalues are occupied, the uppermost filled 'band' is in fact two separate bands overlapping; the matrix element $\langle u_{nk_x} | u_{n(k_x+\delta k_x)} \rangle$ of the periodic parts of the Bloch functions of the highest occupied states at the k points either side of the crossing point therefore vanishes, yielding an infinite $\langle x^2 \rangle_c$. (See Appendix A for details of the calculation of z_N in non-interacting systems.) In this case, therefore, $\langle x^2 \rangle_c$ gives no information about the onset of a metal-insulator transition from the insulating side. Figure 2(c) shows the localization length in the x direction as the y confinement is reduced. The value of $\langle x^2 \rangle_c$ falls slightly as the eigenfunctions spread out more along y, but because the uppermost unoccupied band does not influence the band below, there is no sign of the transition until it happens.

On the other hand, if instead we fill the three lowest bands and adjust ω_x and ω_y until the top of the p_x band touches the next band up (which has the same reflection symmetry as p_x), the states that become degenerate at the band crossing have the same symmetry under reflection in the x-axis. When k_x is exactly zero, the crossing bands have different y-reflection symmetries and cannot mix, but they hybridize and repel each other for other values of k_x. Figures 3(a) and 3(b) show the lowest four

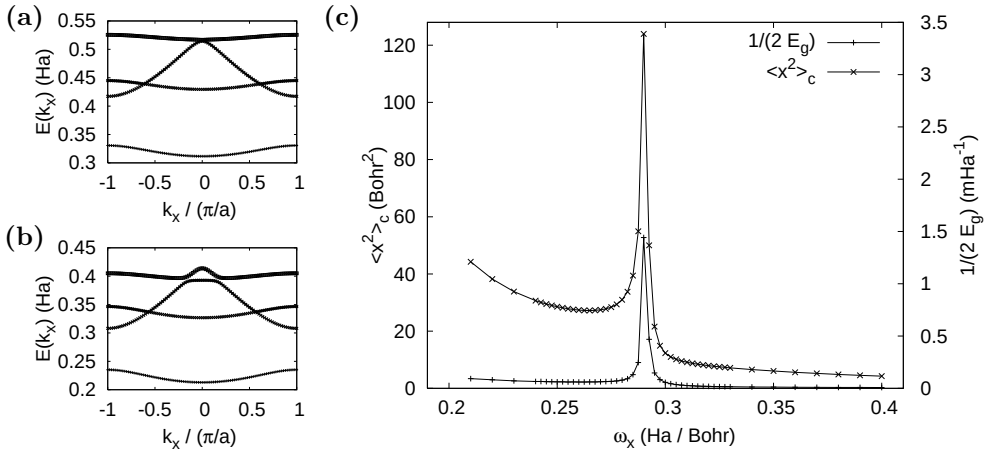

Figure 3. One-dimensional chain of 6-electron dots: **(a)** Energy bands $E(k_x)$ just before band crossing. **(b)** Energy bands $E(k_x)$ shortly after transition **(c)** Localization length $\langle x^2 \rangle_c$ and inverse direct energy gap to lowest unoccupied state $1/(2E_g)$ as ω is reduced.

bands just as the bands touch and shortly after, as ω_x is reduced. The system is never truly metallic, although the gap becomes arbitrarily small at k_x=0. Nevertheless, the rapidly changing nature of the band with k_x means that the overlap integrals $\langle u_{nk_x} | u_{n(k_x+\delta k_x)} \rangle$ become very small around k_x=0, yielding a spike in the localization length near the 'transition', as shown in Fig.3(c).

A simple one-dimensional tight-binding Hamiltonian that models this situation can be constructed by considering only the highest occupied and lowest unoccupied bands before and after the hybridization. The final eigenstates $\psi_{ik}(x) = e^{ikx} u_{ik}(x)$ for $i = 1, 2$ are constructed from a linear combination of basis functions $\chi_{ik}(x)$ which are not eigenstates of the Hamiltonian themselves but have a Bloch-like form with orthogonal periodic parts ϕ_{ik}:

$$\chi_{ik}(x) = \phi_{ik}(x) e^{ikx} \tag{31}$$

When expressed in the basis of the these functions the Hamiltonian matrix for small values of k, must, to produce the system described above, take the form (for an appropriate choice of external potential):

$$\hat{H} = \begin{pmatrix} \Delta + \alpha k^2 & \Gamma k^2 \\ \Gamma k^2 & -\Delta - \beta k^2 \end{pmatrix}, \tag{32}$$

where α and β describe the curvature of the uncoupled Bloch bands and Γ the matrix element between them. Diagonalising this Hamiltonian gives the eigenvalues

$$\epsilon^{\pm} = \frac{(\alpha - \beta)}{2} k^2 \pm \sqrt{\left(\frac{(\alpha + \beta)}{2} k^2 + \Delta \right)^2 + \Gamma^2 k^4} \tag{33}$$

This shows that when $\Delta > 0$, the two bands are separated by a direct band gap of 2Δ at k=0. As the value of Δ reduces, the band gap also reduces. The two bands touch briefly when Δ=0, after which, as Δ becomes negative, they hybridize and repel in the manner shown in Fig. 3(b).

Diagonalising the Hamiltonian also yields the eigenvectors

$$\mathbf{c}^{\pm}(k) = \frac{1}{\sqrt{1+|p^{\pm}(k)|^2}}\Big[p^{\pm}(k),\ 1\Big]\,, \tag{34}$$

where

$$p^{\pm}(k) = \left(\frac{\alpha+\beta}{2\Gamma}+\frac{\Delta}{\Gamma k^2}\right) \pm \sqrt{\left(\frac{\alpha+\beta}{2\Gamma}+\frac{\Delta}{\Gamma k^2}\right)^2+1}\,. \tag{35}$$

The elements of the eigenvectors are the components of the periodic parts $u_k^{\pm}$ of the Bloch eigenstates $\psi_k^{\pm}$ along the basis functions $\phi_{1k}(x)$ and $\phi_{2k}(x)$:

$$u_k^{\pm}(x) = c_1^{\pm}(k)\phi_{1k}(x) + c_2^{\pm}(k)\phi_{2k}(x)\,. \tag{36}$$

Here we make the approximation that the dominant contribution to the localization length comes from the variation of the eigenvectors with k rather than the basis functions themselves. This is equivalent to neglecting the $\frac{\partial\phi_{ik}}{\partial k}$ terms in $\frac{\partial u_{ik}}{\partial k}$. This will inevitably become a valid approximation as $\Delta \to 0$ as the orbitals ϕ_{ik} are largely independent of Δ whereas the functions $p^{\pm}(k)$ vary very rapidly with it around $k = 0$.

Only the lower state is occupied, so substituting the expression for the periodic part $u_k^-(x)$ of the occupied eigenfunction $\psi_k^-(x)$ into Eq. (18) yields, after some algebra,

$$\langle x^2\rangle_c = \frac{a}{2\pi}\int_{-\pi/a}^{\pi/a} \frac{1}{(1+(p^-(k))^2)^2}\left(\frac{\partial p^-(k)}{\partial k}\right)^2 dk\,. \tag{37}$$

For fixed values of α, β and Γ, the scaling behaviour with the gap parameter Δ may be extracted by changing variables to $u = \Delta/k^2$. Noting that the integral is symmetric about $k = 0$, we obtain

$$\langle x^2\rangle_c = \frac{2a}{\pi\sqrt{\Delta}}\int_{\Delta a^2/\pi^2}^{\infty} \frac{u^{3/2}\left(\frac{\partial p^-(u)}{\partial u}\right)^2}{(1+(p^-(u))^2)^2}\,\mathrm{d}u\,. \tag{38}$$

Hence, for small enough values of the gap parameter Δ, since the integrand does not diverge as $u \to 0$, the quadratic spread $\langle x^2\rangle_c \propto \Delta^{-1/2}$. This is roughly consistent with the behaviour seen in Fig.3. However, because of finite size effects and convergence issues, it is proves difficult to obtain enough data close enough to the point where the gap closes to determine if this relationship holds accurately. Additionally, there will be a constant term present due to the variation of the ϕ_{ik} terms with k that will obscure this scaling behaviour until it is negligeable compared to the relevant effect.

5.2. Single dots in a two-dimensional array

This arrangement restores the two-dimensional symmetry and returns to potentials of the type described in Sec. 4, with a square lattice of unit cells each containing a single dot. In this situation, with the potential and the lattice symmetric in x and y, the p_x and p_y bands are degenerate along ΓM. By filling the first three bands and gradually reducing the strength of the confining potential, we can still drive the system through a transition to a metallic state, but this now occurs when the indirect gap above the p bands closes, as can be seen from Fig. 4(a). Because the highest occupied and lowest unoccupied states are well separated in reciprocal space, the occupied states do not change nature or become strongly dependent on $\mathbf{k}$ as the gap closes, and the matrix elements between the periodic parts of the eigenfunctions at neighbouring $\mathbf{k}$ vectors

behave smoothly. The localization length increases as the bands are brought together because the confining potential is being reduced, but it does not diverge on approach to the transition. This emphasises again the importance of the approaching bands being able to 'see' each other if anything is to be observed in $\langle x^2 \rangle_c$.

The Kohn-Sham orbitals determined from this DFT simulation were combined with an optimized 1- and 2-electron Jastrow factor to evaluate energies and localization lengths within the many-electron variational quantum Monte Carlo (VMC) method, using the CASINO program [27]. The variance minimization procedure used to optimize the Jastrow factor resulted in close agreement between the DFT and VMC energies. As a consistency check, we confirmed that localization lengths calculated using VMC trial functions consisting of a Slater determinant of Kohn-Sham orbitals only, with no Jastrow factor, agreed with those obtained using the DFT-based method of Appendix A to within the statistical error of the Monte Carlo simulation. A discussion of the errors associated with the quantum Monte Carlo measurement of z_N can be found in Appendix B.

Figure 4 shows the localization length of this indirect-gap system calculated using both DFT and VMC. As expected, decreasing the confinement by moving from right to left across the figure results in a gradual increase in the localization length, followed by a discontinous jump to an infinite value when the indirect gap closes and some of the bands become partially filled. As discussed in Appendix B, it is difficult to evaluate very small values of z_N (and hence very large localization lengths) using VMC because the statistical errors begin to overwhelm the result. It is clear, however, that the VMC localization length is shorter than the DFT localization length and appears to track it. To the extent that it is possible to judge, it appears that the DFT and VMC localization lengths jump discontinuously to infinity at the same point, presumably because the VMC Slater determinant is constructed using the occupied set of DFT orbitals, which changes discontinuously when the DFT gap closes. If the orbitals in the VMC determinant had been chosen to minimize the VMC energy, the VMC transition would presumably have occurred at a smaller value of ω.

The difference between the localization lengths obtained in DFT and VMC has a simple interpretation in terms of the size of the correlation hole produced by including a Jastrow factor. In systems with open boundary conditions, Resta [24] showed that the localization length could be related (in a considerably simpler manner than is possible when periodic boundary conditions are used) to the form of the exchange-correlation hole $n_{\mathrm{xc}}(\mathbf{r}, \mathbf{r}')$:

$$\langle r_\alpha^2 \rangle = \frac{-1}{2N} \int \mathrm{d}\mathbf{r} \int \mathrm{d}\mathbf{r}' (r_\alpha - r'_\alpha)^2 n(\mathbf{r}) n_{\mathrm{xc}}(\mathbf{r}, \mathbf{r}') \; . \tag{39}$$

In DFT, where the wavefunction is a single Slater determinant, the exchange-correlation hole has to be replaced by the exchange hole (calculated using the DFT orbitals):

$$\langle r_\alpha^2 \rangle_{\mathrm{x}} = \frac{-1}{2N} \int \mathrm{d}\mathbf{r} \int \mathrm{d}\mathbf{r}' (r_\alpha - r'_\alpha)^2 n(\mathbf{r}) n_{\mathrm{x}}(\mathbf{r}, \mathbf{r}') \; . \tag{40}$$

Assuming, as is normally the case, that the one-electron density $n(\mathbf{r})$ is almost the same in the correlated calculation as in the uncorrelated calculation, this gives

$$\langle r_\alpha^2 \rangle_{\mathrm{x}} - \langle r_\alpha^2 \rangle \approx \frac{1}{2N} \int \mathrm{d}\mathbf{r}\, n(\mathbf{r}) \int \mathrm{d}\mathbf{r}''\, (r''_\alpha)^2\, n_c(\mathbf{r}, \mathbf{r} + \mathbf{r}'') \; . \tag{41}$$

The correlation hole $n_c(\mathbf{r}, \mathbf{r} + \mathbf{r}'')$ is negative when $|\mathbf{r}''|$ is small but integrates to zero, implying that it must be mostly positive when $|\mathbf{r}''|$ is large. The $(r''_\alpha)^2$ factor in

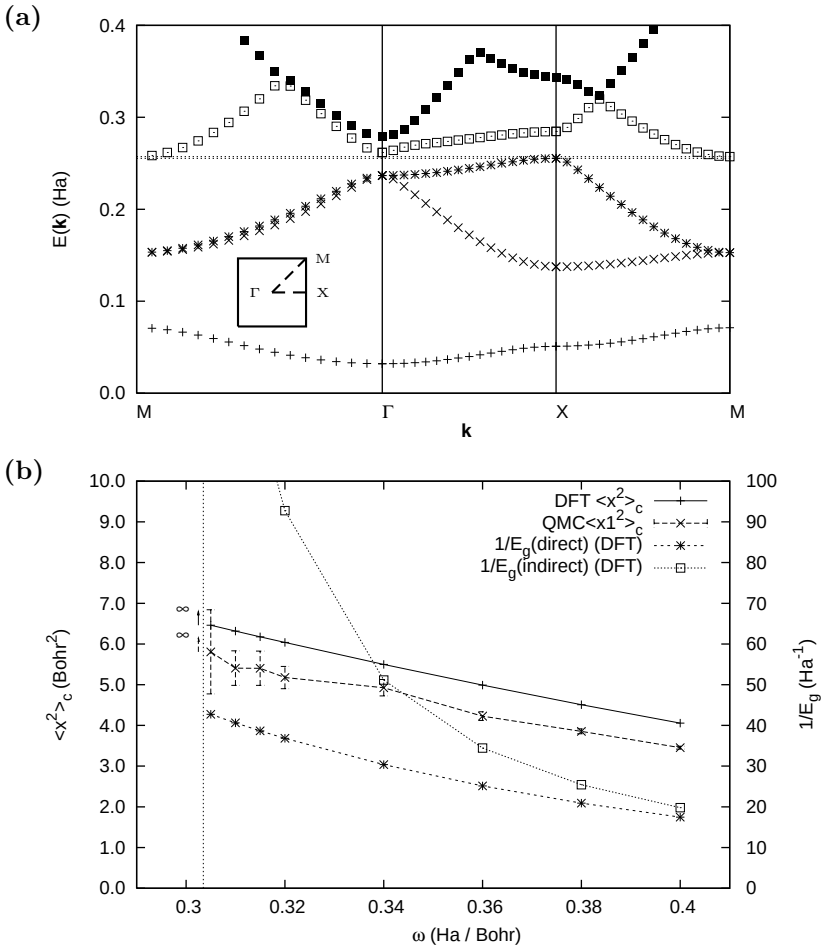

Figure 4. (a) Energy bands $E(\mathbf{k})$ along the high symmetry lines (inset: Brillouin zone of two-dimensional square lattice). Dotted lines denote the Fermi level. **(b)** Localization length $\langle x^2 \rangle_c$ in DFT and QMC as the dot confinement ω is varied (left scale). Inverse DFT direct and indirect energy gaps (right scale). Below 0.305 Ha/Bohr the system is metallic so $\langle x^2 \rangle_c$ becomes abruptly infinite. No divergence is seen while approaching the transition from the region of stronger confinement.

Eq. (41) lends weight to the large $|\mathbf{r}''|$ region of the integral, and so one would expect $\langle r_\alpha^2 \rangle_\mathrm{x} - \langle r_\alpha^2 \rangle$ to be positive in most cases. In other words, the VMC calculation of the localization length, which includes some of the effects of correlation via the Jastrow factor, ought to yield a smaller result than the exchange-only DFT calculation. Indeed, as seen from the difference between the DFT and VMC results for $\langle x^2 \rangle_c$ in Fig. 4(b), the left-hand side of Eq. (41) in this system has a value of around 0.7, implying that the root-mean-square radius of the correlation hole is 0.8 to 0.9 Bohr.

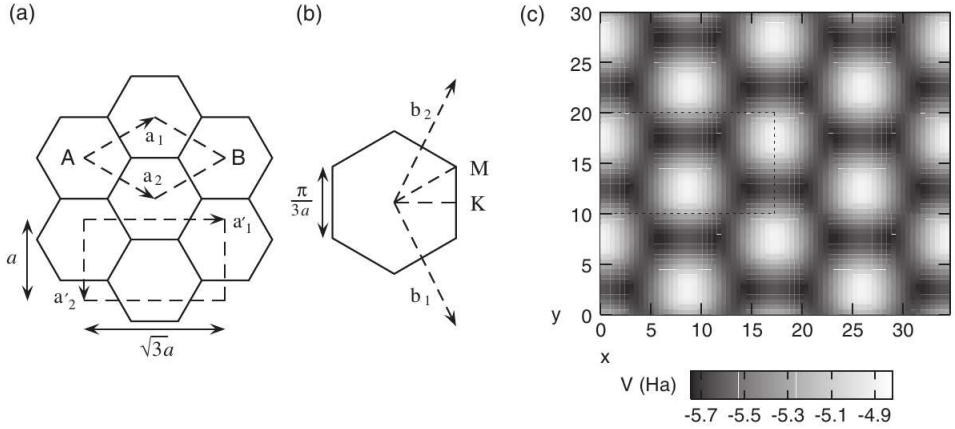

Figure 5. **(a)** The structure of the graphene-like model, showing the lattice vectors $\mathbf{a}_1$, $\mathbf{a}_2$ of the primitive cell (top), the lattice vectors $\mathbf{a}'_1$, $\mathbf{a}'_2$ of the larger rectangular cell used for simplicity (bottom), and the sites A and B on which the potential can be varied. **(b)** The Brillouin zone of the graphene-like model showing the reciprocal lattice vectors $\mathbf{b}_1$, $\mathbf{b}_2$ and the high symmetry $\mathbf{k}$-points $\mathbf{K}$, $\mathbf{M}$ and $\mathbf{\Gamma}$. **(c)** The external potential of the graphene-like model for $a = 10$, $V_d = 3$, $\rho = 5$, and $\Delta = 0$. The dotted line encloses one rectangular unit cell.

5.3. Graphene structure in a hexagonal lattice

The hexagonal lattice model of a graphene sheet provides a realistic example in which a direct gap can be tuned down to zero. Real graphene consists of an equilateral triangular (hexagonal) two-dimensional lattice with a basis of two carbon atoms, labelled A and B in Fig. 5(a), and four valence electrons per atom. Three electrons per atom form strong bonds with their nearest neighbours, leaving the electronic properties dominated by the one electron per atom in the π bonds. These form a bonding π band and and anti-bonding π^* band. A tight-binding analysis involving just these bands, as described in [25, 26], demonstrates the main features of the bandstructure: the two electrons per primitive cell fill the π band, which touches the π^* band at the corners of the hexagonal Brillouin zone, labelled $\mathbf{K}$ in Fig. 5(b). Graphene is thus a semiconductor with a zero gap, and has interesting transport properties caused by the zero density of states at the Fermi level. Since the π band is fully occupied, its Wannier functions might be expected to be localized; on the other hand, since the band gap is zero, the upper bound on the localization length provided by the conductivity formula of Souza, Wilkens and Martin (Eq. (52) of [7]) is infinite.

If the potential is modified so that the energies of the two sites in the primitive cell are no longer equivalent, a gap opens up at the Fermi energy and grows in proportion to the difference of the on-site energies. We model this by placing Gaussian dots of the form

$$V_A(\mathbf{r}) = -V_d \exp(-|\mathbf{r} - \mathbf{r}_A|^2/\rho^2) \tag{42}$$

$$V_B(\mathbf{r}) = -(1 + \Delta)V_d \exp(-|\mathbf{r} - \mathbf{r}_B|^2/\rho^2) \tag{43}$$

on the B sites. Figure 5 shows the form of this potential when $\Delta = 0$.

At finite Δ there is an energy gap, caused by the attraction of the electrons to the lower-energy B sites. As $\Delta \to 0$, the energy gap reduces to zero and the localization

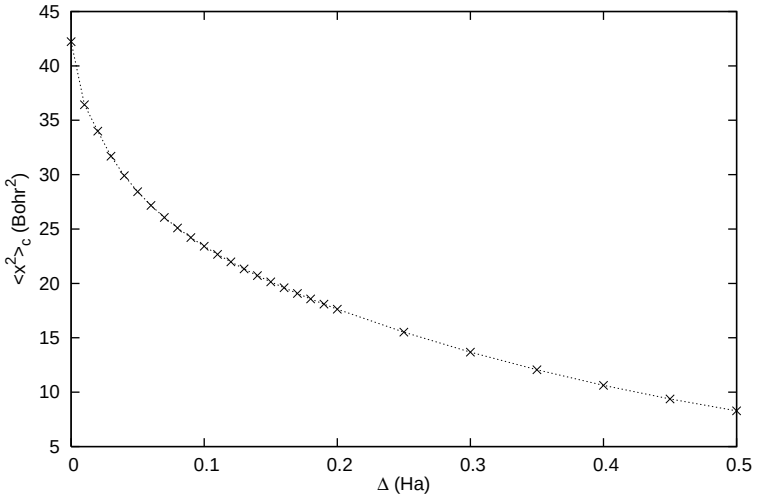

Figure 6. Localization length $\langle x^2 \rangle_c$ as Δ is reduced to 0, at which point there is a transition to a semimetallic state. Available system sizes up to the $N_k = 36 \times 36$ system shown here are insufficient to resolve whether the localization length is truly diverging as the semimetallic state is approached. Even for $\Delta = 0$ a finite value of $\langle x^2 \rangle_c$ is observed at all practical system sizes.

length increases, as shown in Fig. 6. The value of z_N at $\Delta = 0$ remains non-zero (and hence the localization length remains finite) for all practical system sizes. It is unclear whether the touching of the valence and conduction bands at a single point in k space is sufficient to force z_N to tend to zero as the system size tends to infinity.

6. Conclusions

This paper began by offering a variation on previous presentations of the theory of localization lengths in periodic systems, highlighting the connection to many-body Wannier functions. By considering the decomposition of the many-body wavefunction of an insulator into localized clusters of correlated Wannier functions that do not overlap in configuration space, it also provided a new justification of the standard single-point formulae used in the modern theory of polarization.

Our calculations of localization lengths in model quasi-one-dimensional periodic and two-dimensional periodic systems revealed several new effects. In particular, they showed how the symmetry properties of the bands that cross at an insulator-to-metal transition determine whether or not the localization length diverges smoothly or jumps suddenly to infinity. Our results for a range of direct-gap and indirect-gap insulator-metal transitions in one and two dimensions show that the localization length does not diverge unless the gap that is closing is direct and the two bands have the same symmetry at the crossing point. Since bands of the same symmetry do not in general cross, this suggests that it will be difficult to observe diverging localization lengths associated with insulator-to-metal transitions in real systems.

We have shown using variational Monte Carlo simulations that localization lengths in correlated systems behave in broadly the same way as in one-electron methods. Despite the many-particle nature of the operator that yields z_N, the localization length in VMC is largely a one-electron property, reflecting the nature

of the one-electron orbitals used to construct the determinantal part of the Slater-Jastrow trial function. In strongly correlated solids, where the simple Slater-Jastrow form may be inadequate, more interesting behaviour may be observed. Finally, we explained how the difference between the localization length calculated in DFT and that calculated using a fully correlated method provides an approximate measure of the range of the correlation hole.

Appendix A. Evaluation of z_N in a Plane-Wave Basis

Localization lengths are calculated from the one-electron Bloch functions using the method described in [2]. In this approach, the many-body wavefunction $\widetilde{\Psi}$ in Eq. (29) is a Slater determinant of single-particle orbitals, and the expectation value $\left\langle\widetilde{\Psi}\middle|e^{-i\delta\mathbf{k}_\alpha\cdot\widetilde{\mathbf{X}}}\middle|\widetilde{\Psi}\right\rangle$ is expressed as $\left\langle\widetilde{\Psi}|\widetilde{\Phi}\right\rangle$, where $\widetilde{\Phi}$ is a Slater determinant of the orbitals $\psi_{n\mathbf{k}}(\mathbf{r}_j)$ of $\widetilde{\Psi}$, each multiplied by $e^{-i\delta\mathbf{k}_\alpha\cdot\mathbf{r}_j}$. The overlap of two Slater determinants is a determinant of the overlaps of the individual orbitals, and as shown in [2], the only terms $\langle\psi_{n\mathbf{k}}|e^{i\delta\mathbf{k}_\alpha\cdot\mathbf{r}}|\psi_{n'\mathbf{k}'}\rangle$ of this determinant which survive the integration over the whole system are those for which $\mathbf{k}' = \mathbf{k} + \delta\mathbf{k}_\alpha + \mathbf{G}$, where $\mathbf{G}$ is a primitive reciprocal lattice vector (which may be zero). This makes the matrix very sparse indeed. The determinant can be factorized as

$$\left\langle\widetilde{\Psi}\middle|e^{-i\delta\mathbf{k}_\alpha\cdot\widetilde{\mathbf{X}}}\middle|\widetilde{\Psi}\right\rangle = \prod_{\mathbf{k}} \det S(\mathbf{k}) \;, \tag{A.1}$$

where $S_{nn'}(\mathbf{k})$ is a matrix of overlaps between the periodic parts of the Bloch functions at points $\mathbf{k}$ and $\mathbf{k} + \delta\mathbf{k}_\alpha + \mathbf{G}$. If both $\mathbf{k}$ and $\mathbf{k} + \delta\mathbf{k}_\alpha$ lie within the Brillouin zone (so that $\mathbf{G} = \mathbf{0}$), then

$$S_{nn'}(\mathbf{k}) = \langle u_{n\mathbf{k}}|\; u_{n'\mathbf{k}+\delta\mathbf{k}_\alpha}\rangle \;. \tag{A.2}$$

If $\mathbf{k}$ lies inside the Brillouin zone but $\mathbf{k} + \delta\mathbf{k}_\alpha$ lies outside, then

$$\begin{aligned} S_{nn'}(\mathbf{k}) &= \langle\psi_{n\mathbf{k}}|\, e^{-i\delta\mathbf{k}_\alpha\cdot\mathbf{r}}\,|\psi_{n'\mathbf{k}+\delta\mathbf{k}_\alpha-\mathbf{G}}\rangle \\ &= \langle u_{n\mathbf{k}}|\, e^{-i\mathbf{G}\cdot\mathbf{r}}\,|u_{n'\mathbf{k}+\delta\mathbf{k}_\alpha-\mathbf{G}}\rangle \;, \end{aligned} \tag{A.3}$$

where $\mathbf{G}$ is chosen such that $\mathbf{k} + \delta\mathbf{k}_\alpha - \mathbf{G}$ lies inside the Brillouin zone (because that was the state included in the original Slater determinant). In a plane-wave basis, the matrix elements can be evaluated directly from the plane-wave coefficients using Parseval's relation, as:

$$S_{nn'}(\mathbf{k}) = \sum_{\mathbf{G}'} c^*_{n\mathbf{k}}(\mathbf{G}')c_{n'\mathbf{k}+\delta\mathbf{k}_\alpha-\mathbf{G}}(\mathbf{G}'+\mathbf{G}) \;, \tag{A.4}$$

where $\mathbf{G}$ is the reciprocal lattice vector that brings $\mathbf{k}+\delta\mathbf{k}_\alpha$ back into the first Brillouin zone if required. This expression allows very efficient calculation of z_N and thus the localization lengths.

Appendix B. Statistical Errors on Localization Lengths within QMC

The form of Eq. (29) is well suited to evaluating the localization length within the framework of quantum Monte Carlo [22] and has been applied previously [9, 13]. As with the evaluation of any quantity with Monte Carlo methods, there is an associated statistical error and some examination of its behaviour is required, especially in cases where the localization length is large. In the simplest QMC technique, variational

Monte Carlo, expectation values are evaluated by using the Metropolis algorithm to sample "configurations" $C = (\mathbf{r}_1, \mathbf{r}_2, \ldots, \mathbf{r}_N)$ of electron positions distributed according to the probability distribution defined by the trial wavefunction. The expectation value of the many-body phase operator in Eq. (29) is evaluated by taking the sum of the electron coordinates $\mathbf{X}(C) = \mathbf{r}_1 + \mathbf{r}_2 + \ldots + \mathbf{r}_N$ for each sampled configuration C, calculating the quantity

$$z_N(C) = e^{-i\delta\mathbf{k}_\alpha \cdot \mathbf{X}(C)} \; , \tag{B.1}$$

and averaging over a sufficient number M of statistically independent configurations to obtain:

$$\overline{z}_N = \frac{1}{M} \sum_{m=1}^{M} z_N(C_m) \; . \tag{B.2}$$

As M tends to infinity, the sample mean $\overline{z}_N$ tends to z_N and the localization length can be obtained from the formula

$$\langle r_\alpha^2 \rangle_c \; = \; -\frac{1}{N} \frac{\widetilde{A}_\alpha^2}{(2\pi)^2} \ln |z_N|^2 \; \approx \; -\frac{1}{N} \frac{\widetilde{A}_\alpha^2}{(2\pi)^2} \ln |\overline{z}_N|^2 \; . \tag{B.3}$$

The complication is that $z_N(C_m)$ is a complex number whose modulus is always unity but whose mean z_N is very small if the localization length is large. To ensure the result is not swamped by the statistical error $\sigma_{|\overline{z}_N|}$ in $|\overline{z}_N|$, the number of configurations M must be large enough that $\sigma_{|\overline{z}_N|} \ll |z_N|$.

The error in the localization length can be estimated as follows. Given a complex random variable such as $\overline{z}_N = \overline{x}_N + i\,\overline{y}_N$, where $\overline{x}_N$ and $\overline{y}_N$ are statistically independent real random variables with population mean values x_N and y_N, $\sigma_{\overline{x}_N} \ll x_N$, and $\sigma_{\overline{y}_N} \ll y_N$, it is easy to show that

$$\sigma_{\ln(|\overline{z}_N|^2)} = \sigma_{\ln(\overline{x}_N^2 + \overline{y}_N^2)} \approx \frac{\sqrt{4x_N^2 \sigma_{\overline{x}_N}^2 + 4y_N^2 \sigma_{\overline{y}_N}^2}}{x_N^2 + y_N^2} \; . \tag{B.4}$$

Assuming that the M individual readings $x_N(C)$ and $y_N(C)$ used to calculate the sample mean values $\overline{x}_N$ and $\overline{y}_N$ are uncorrelated, $\sigma_{\overline{x}_N}^2 = \sigma_{x_N}^2/M$ and $\sigma_{\overline{y}_N}^2 = \sigma_{y_N}^2/M$, so

$$\sigma_{\ln(|\overline{z}_N|^2)} \approx \frac{\sqrt{4x_N^2 \sigma_{x_N}^2 + 4y_N^2 \sigma_{y_N}^2}}{\sqrt{M}(x_N^2 + y_N^2)} \; , \tag{B.5}$$

where σ_{x_N} and σ_{y_N} are the errors in a single reading $x_N(C)$ or $y_N(C)$. (For metallic systems with a small number of electrons in the conduction band or holes in the valence band, the values of $z_N(C)$ from configuration to configuration are very strongly correlated and it takes many more than M VMC steps to accumulate M uncorrelated VMC samples. This occurs because the values of $z_N(C)$ depend strongly on the current positions of the "extra" or "missing" electrons in the cell.) The error in a single reading of z_N can be estimated by assuming its mean is in fact zero and that its possible values are distributed uniformly around the unit circle in the complex plane, so that

$$\sigma_{x_N}^2 = \sigma_{y_N}^2 = \frac{1}{2\pi} \int_0^{2\pi} \cos^2\theta \, \mathrm{d}\theta = \frac{1}{2} \; . \tag{B.6}$$

Finally, combining Eqs. (B.5) and (B.6) with Eq. (B.3), we obtain

$$\sigma_{\langle r_\alpha^2\rangle_c} \;=\; \frac{\widetilde{A}_\alpha^2\sqrt{2}}{(2\pi)^2 N|z_N|\sqrt{M}}\;. \tag{B.7}$$

Since $\langle r_\alpha^2\rangle_c = -\kappa \ln|z_N|^2$, where κ is a constant, $|z_N|$ approaches zero like $e^{-\langle r_\alpha^2\rangle_c/2\kappa}$ as $\langle r_\alpha^2\rangle_c$ tends to infinity, as we might expect at an appropriate type of insulator-to-metal transition. It then requires exponentially longer runs to achieve a given error bar on $\langle r_\alpha^2\rangle_c$.

References

[1] C. Brouder, G. Panati, M. Calandra, C. Mourougane, and N. Marzari, Phys. Rev. Lett. **98**, 046402 (2007).
[2] C. Sgiarovello, M. Peressi, R. Resta, Phys. Rev. B **64**, 115202 (2001).
[3] W. Kohn, Phys. Rev. **133**, A171 (1964).
[4] R. D. King-Smith and D. Vanderbilt, Phys. Rev. B **47**, R1651 (1993)
[5] D. Vanderbilt and R. D. King-Smith, Phys. Rev. B **48**, 4442 (1993).
[6] R. Resta, S. Sorella, Phys. Rev. Lett. **82**, 370 (1999)
[7] I. Souza, T. Wilkens, R. Martin, Phys. Rev. B **62**, 1666 (2000).
[8] M. Veithen, X. Gonze, and Ph. Ghosez, Phys. Rev. B **66**, 235113 (2002).
[9] P. Umari, A. J. Willamson, G. Galli, and N. Marzari, Phys. Rev. Lett **95**, 207602 (2005).
[10] P. Umari, X. Gonze, A. Pasquarello, Phys. Rev. B **69**, 235102 (2004).
[11] N. Marzari and D. Vanderbilt, Phys. Rev. B **56**, 12847 (1997).
[12] R. Resta, Ferroelectrics **136**, 51 (1992).
[13] T. Wilkens and R. Martin, Phys. Rev. B **63**, 235108 (2001).
[14] A. Filippetti and N. Spaldin, Phys. Rev. B **68**, 045111 (2003)
[15] W. Kohn, Phys. Rev. **115**, 809 (1959).
[16] W. Kohn and J. R. Onffroy, Phys. Rev. B **8**, 2485 (1973).
[17] G. H. Wannier, Phys. Rev. **52**, 191 (1937).
[18] E.I. Blount, Solid State Phys. **13**, 306 (1962).
[19] G. Rajagopal, R.J. Needs, A. James, S. D. Kenny, and W. M. C. Foulkes, Phys. Rev. B **51**, 10591 (1995).
[20] G. Ortiz and R.M. Martin, Phys. Rev. B **49**, 14202 (1994).
[21] C. Attaccalite, S. Moroni, P. Gori-Giorgi, and G. Bachelet, Phys. Rev. Lett. **88**, 256601 (2002).
[22] W. M. C. Foulkes, L. Mitas, R. J. Needs and G. Rajagopal, Rev. Mod. Phys. 73, 33 (2001).
[23] R. Resta, Phys. Rev. Lett. 80, 1800 (1998).
[24] R. Resta, Phys. Rev. Lett. 96, 137601 (2006).
[25] P. R. Wallace, Phys. Rev. **71**, 622 (1947).
[26] R. Saito, G. Dresselhaus, M. S. Dresselhaus, *Physical Properties of Carbon Nanotubes* (Imperial, London, 1998).
[27] R.J. Needs, M.D. Towler, N.D. Drummond and P.R.C. Kent (2004) CASINO Version 2.0 User Manual (Cambridge: University of Cambridge)